Topological orbital magnetization and emergent Hall effect of an atomic-scale spin lattice at a surface

M. Hoffmann,[1,*] J. Weischenberg,[2] B. Dupé,[1] F. Freimuth,[2] P. Ferriani,[1] Y. Mokrousov,[2] and S. Heinze[1]

[1]*Institute of Theoretical Physics and Astrophysics, Christian-Albrechts University of Kiel, Leibnizstrasse 15, D-24098 Kiel, Germany*
[2]*Peter Grünberg Institut and Institute for Advanced Simulation, Forschungszentrum Jülich and JARA, 52425 Jülich, Germany*

We predict the occurrence of a novel type of atomic-scale spin lattice in an Fe monolayer on the Ir(001) surface. Based on density functional theory calculations we parametrize a spin Hamiltonian and solve it numerically using Monte Carlo simulations. We find the stabilization of a three-dimensional spin structure arranged on a (3×3) lattice. Despite an almost vanishing total spin magnetization we predict the emergence of orbital magnetization and large anomalous Hall effect, to which there is a significant topological contribution purely due to the real space spin texture at the surface.

Localized stable spin textures such as skyrmions or chiral domain walls have attracted much attention recently due to their unique topological and transport properties [1–3] and potential applications in spintronics [4–7]. A key ingredient for their occurrence is the Dzyaloshinskii-Moriya (DM) interaction [8,9], which arises due to spin-orbit interaction in systems with broken inversion symmetry, as in the bulk of noncentrosymmetric crystals or at surfaces and interfaces. Hall effects play an important role in these systems. For instance, the spin-orbit torque originating from the spin Hall effect drives the motion of chiral domain walls in ultrathin films very efficiently and very high speeds have been reported [2,3]. The topological Hall effect (THE), defined as the contribution to the Hall resistivity due to chiral spin texture, serves as one of the main tools to pinpoint the skyrmion phase in the phase diagram of bulk alloys such as MnSi or FeGe [10–15].

The discovery of a nanoskyrmion lattice in an Fe monolayer (ML) on the Ir(111) surface [16] opened an entirely new class of materials for magnetic skyrmions—transition-metal films and interfaces—which are of prime interest for spintronic devices [6]. Such systems have the benefit of allowing us to engineer the skyrmion properties by film composition and structure [17,18] and to address individual magnetic skyrmions [16,19–21]. However, very little is known both experimentally and theoretically about Hall effects in such complex nanometer-scale spin textures at surfaces and interfaces. Another open question concerns the diversity of the class of topologically distinct spin textures which can arise in these systems. In this respect an appealing idea is the realization of antiferromagnetic skyrmions [22,23], which are weakly susceptible to external fields and promise faster dynamics [24,25]; however, real systems are missing so far.

Here, we predict a new type of a complex spin lattice at a surface which both exhibits unique topological and transport properties and may serve as a possible seed structure for sought-after antiferromagnetic skyrmions [22,23]. Namely, using density functional theory (DFT) and Monte Carlo techniques, we find a complex three-dimensional spin structure with angles close to 120° between adjacent spins on a (3×3)

lattice for an Fe ML on Ir(001) [26]. In contrast to systems explored so far for magnetic skyrmions the local exchange interaction is antiferromagnetic in this system, and it can be considered as an antiferromagnetic twin of the nanoskyrmion spin structure formed in the Fe ML on Ir(111) [16]. The nontrivial topological nature of the novel spin lattice with almost compensated total magnetization manifests in the large anomalous Hall effect (AHE). Moreover, taking the obtained (3×3) spin lattice as an example, we show that complex real-space topology of spin textures at metallic transition-metal surfaces can completely replace the spin-orbit interaction in giving rise to large AHE and orbital magnetization—phenomena, traditionally viewed as key manifestations of spin-orbit interaction in solids.

Nanoscale spin textures at transition-metal interfaces [16,17,27,28] can be treated employing a Hamiltonian on the discrete atomic lattice

$$
\begin{aligned}
H = &- \sum_{ij} J_{ij}(\mathbf{M}_i \cdot \mathbf{M}_j) - \sum_{ij} \mathbf{D}_{ij} \cdot (\mathbf{M}_i \times \mathbf{M}_j) \\
&- \sum_{ijkl} K_{ijkl}[(\mathbf{M}_i \cdot \mathbf{M}_j)(\mathbf{M}_k \cdot \mathbf{M}_l) + \cdots] \\
&- \sum_{ij} B_{ij}(\mathbf{M}_i \cdot \mathbf{M}_j)^2 + \sum_i K_\perp (M_i^z)^2,
\end{aligned} \quad (1)
$$

which describes the exchange interaction (J_{ij}), the DM interaction ($\mathbf{D}_{ij}$), the four-spin interaction (K_{ijkl}), and the biquadratic exchange (B_{ij}) between the magnetic moments $\mathbf{M}_i$ of atoms at sites $\mathbf{R}_i$ as well as a uniaxial magnetocrystalline anisotropy ($K_\perp$). The interplay of these interactions can result in complex noncollinear spin structures. The nanoskyrmion lattice of Fe/Ir(111) arises due to the weakened ferromagnetic exchange and is enforced by the DM and the four-spin interaction [16]. A single atomic Pd overlayer on Fe/Ir(111) strengthens the ferromagnetic exchange [17] such that individual magnetic skyrmions with a diameter of a few nanometers can be realized [21]. Therefore, an understanding of the relative strength of the competing interactions is essential to tailor skyrmions with desired properties in such type of systems by interface engineering [18].

For the Fe ML on Ir(001), we used DFT to obtain the parameters for the Hamiltonian given by Eq. (1). We
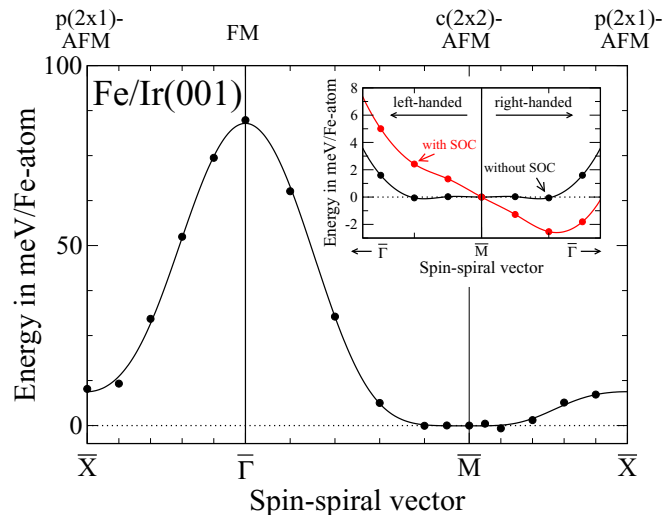
---

*hoffmann@theo-physik.uni-kiel.de

FIG. 1. (Color online) Energy dispersion of homogeneous flat spin spirals for Fe/Ir(001). The energies $E(\mathbf{q})$ (filled circles) are calculated via DFT along the high-symmetry lines of the two-dimensional Brillouin zone and given with respect to the $c(2 \times 2)$ antiferromagnetic state. The solid lines are fits to the Heisenberg model with up to sixth-nearest neighbors [44]. The inset shows the energy dispersion close to the $\bar{M}$ point for left- and right-rotating spirals including SOC, i.e., the effect of the DM interaction.

applied the projector augmented wave (PAW) method [29] as implemented in the VASP code [30,31]. Computational details are given in the Supplemental Material [32] (which refers to Refs. [16,29,30,33–43]).

To determine the exchange constants J_{ij}, we have considered flat spin spirals in which the magnetic moments are confined in a plane with a constant angle between moments at adjacent lattice sites propagating along high-symmetry directions of the surface. Such a spin spiral can be characterized by a wave vector $\mathbf{q}$ from the two-dimensional Brillouin zone (BZ) and the magnetic moment of an atom at site $\mathbf{R}_i$, given by $\mathbf{M}_i = M(\sin(\mathbf{q}\mathbf{R}_i), \cos(\mathbf{q}\mathbf{R}_i), 0)$ with the size of the magnetic moment M.

The calculated energy dispersion $E(\mathbf{q})$ of spin spirals for Fe/Ir(001) is displayed in Fig. 1. At the high-symmetry points we obtain collinear spin structures: the ferromagnetic state at $\bar{\Gamma}$, the $c(2 \times 2)$ antiferromagnetic state at $\bar{M}$, and the $p(2 \times 1)$ antiferromagnetic state at $\bar{X}$. Clearly, the $c(2 \times 2)$ antiferromagnetic state is lowest in energy among the considered collinear states in agreement with previous DFT studies [45]. The energy dispersion is very flat in the vicinity of the $\bar{M}$ point due to the frustration of exchange interactions. A fit to the Heisenberg model, i.e., the first term in Eq. (1), with J_{ij}'s up to sixth-nearest neighbors [44] leads to an excellent description as shown by the solid line in Fig. 1 [46].

Note that the energy dispersion of Fe/Ir(001) is almost inverted with respect to Fe/Ir(111) where the energy dispersion is flat around the $\bar{\Gamma}$ point, i.e., the ferromagnetic state [16,47]. Therefore, we can also expect complex three-dimensional spin structures to occur here but of different type due to the nearest-neighbor antiferromagnetic exchange [37,48].

By taking spin-orbit coupling (SOC) into account, we can determine the magnetocrystalline anisotropy energy (MAE)

defined as the energy difference between configurations with different orientation of the magnetization. For the collinear state of lowest energy, i.e., the $c(2 \times 2)$ antiferromagnetic state, we found an easy out-of-plane axis with a MAE of $K_\perp = -0.25$ meV.

At a surface SOC also induces the DM interaction [49,50]. In order to determine its strength, we have calculated the total energy of a $120°$ spin spiral along the $\overline{\Gamma M}$ direction in a (3×1) supercell including SOC both with a left-handed and a right-handed rotational sense. We find that spin spirals with a right-handed rotational sense are lower by 7.3 meV/Fe atom. This energy difference allows us to calculate the value of the DM interaction within the nearest-neighbor approximation which results in a value of $D_1 = 1.5$ meV. Including the DM interaction into the energy dispersion of spin spirals leads to an energy minimum at an angle of about $138°$ between adjacent spins as shown in the inset of Fig. 1.

From the energy dispersion of spin spirals, only the Heisenberg-type exchange can be obtained. The impact of higher-order spin interactions can be determined by considering superposition states of two spin spirals. If only Heisenberg-type exchange played a role all of these spin states would be degenerate in energy. However, our DFT calculations show considerable energy differences on the order of a few meV/Fe-atom (see Supplemental Material [32]). From these calculations, we determine that the nearest-neighbor four-spin, $K_{4\text{spin}}$, and biquadratic, B, interaction fulfill the condition $2K_{4\text{spin}} + B = 0.7$ meV.

The energy functional Eq. (1) with the parameters from DFT can be minimized using Monte Carlo simulations based on the Metropolis algorithm. We have chosen a spin lattice of (66×66) spins and used periodic boundary conditions. We have checked the impact of the lattice size and of using open boundary conditions and found no effect on the obtained ground state. In order to explore the impact of the higher-order spin interactions, which are not univocally determined by our DFT calculations as discussed above, we have chosen different values of B and $K_{4\text{spin}}$ that are in accordance with the condition given above. We changed the value of the four-spin interaction in steps of 0.1 meV and the biquadratic interaction and J_3 were modified accordingly [44].

We found three different types of ground states depending on the value of $K_{4\text{spin}}$ as shown in Fig. 2. A large biquadratic interaction results in a so-called up-up-down-down (*uudd*) state since a collinear alignment of neighboring spins is preferred. However, if the biquadratic interaction is reduced we find an atomic-scale noncollinear (3×3) spin lattice that is stabilized by the four-spin term. For a value of $K_{4\text{spin}} > -0.4$ meV the four-spin term cannot couple the spin spirals and we obtain a spin spiral ground state with an angle of about $140°$ between adjacent spins.

As shown in Fig. 2, the novel (3×3) spin lattice can occur for a large range of values of the four-spin interaction. Its spin structure is shown in Fig. 3. The spins at the corners of the unit cell point upwards perpendicular to the surface while the spins along the sides rotate with an angle of $\approx 123°$ from the surface normal. The four spins in the center of the cell point towards the corners and with an angle of $\approx 22°$ out of the film plane.
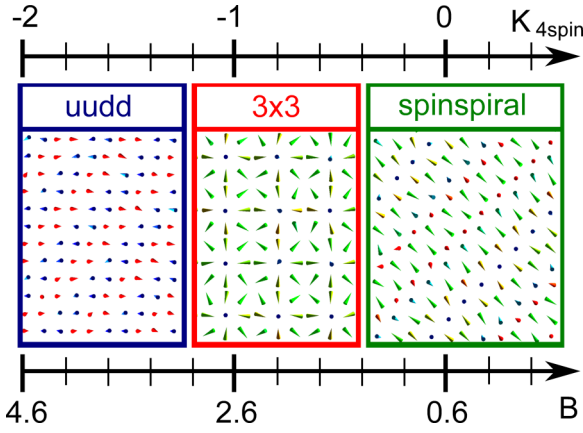
FIG. 2. (Color online) Spin structures of lowest energy obtained via Monte Carlo simulations as a function of the strength of the four-spin interaction. The biquadratic interaction is changed according to the condition $2K_{4spin} + B = 0.7$ meV from the DFT calculations. The sketches only display a small section of the actually simulated spin lattice. Units in the figure are in meV.

The occurrence of this three-dimensional spin structure can be understood from the interplay of the different interactions. The combination of exchange and DM interaction leads to a spin spiral with an angle of approximately 120° between adjacent spins and thus a periodicity of 3 atoms (cf. Fig. 1). For Fe biatomic chains on the (5×1) reconstructed Ir(001) surface, such a spin spiral state has been experimentally observed [20]. In the Fe monolayer on Ir(001), the four-spin interaction can couple these spin spirals into a square lattice. Note that there is an opposite rotational sense of the spin rotation along the side and the diagonal of the unit cell. This results from the antiferromagnetic exchange coupling between nearest neighbors which is stronger than the DM interaction that would prefer a unique rotational sense along both directions.
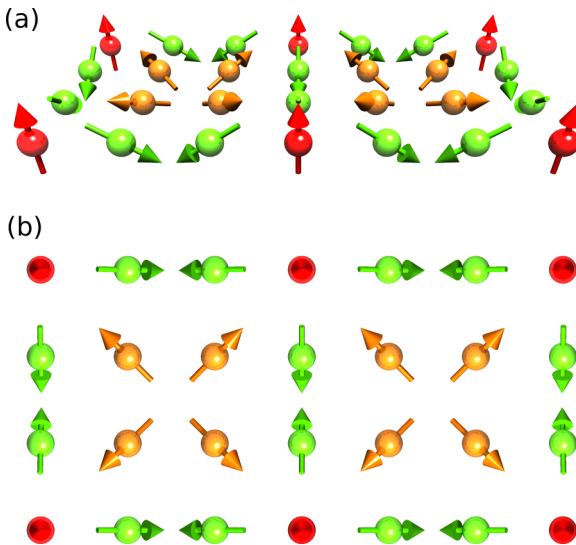
Due to the competition of DMI and Heisenberg exchange, the spin lattice is extremely stable in an external magnetic field and cannot be destroyed up to 80 T as found in our MC simulations. The transition temperature to the paramagnetic state is obtained at approximately 60 K. We propose that tuning the antiferromagnetic exchange interaction in this system by interface engineering [17,18] may open the route to antiferromagnetic skyrmions.

The topological Hall effect in complex large-scale magnetic structures is normally described assuming the adiabatic view-point of infinitesimally slowly varying spin texture [1]. For skyrmions, the topological Hall resistivity can be factorized into the product of an emergent magnetic field, which is the direct consequence of the nonzero topological charge, and the topological Hall coefficient R^{top}, which can be determined from the electronic structure of the ferromagnetic crystal [10,13,14]. On the other side of the length scale, the chirality-driven contribution to the AHE has been predicted and observed in bulk strongly frustrated correlated oxides and bulk antiferromagnets, which exhibit noncollinear magnetic order on the scale of 1 nm [51–58].

To investigate whether the (3×3) spin texture results in nontrivial transport properties, we compute from first principles [32] the intrinsic Berry curvature contribution to the xy component of the anomalous Hall conductivity (AHC) in the system $\sigma_{3\times3}^{AH} = \frac{e^2\hbar}{(2\pi)^2} \int_{BZ} \Omega_{xy}(\mathbf{k}) d\mathbf{k}$ [59], where

$$\Omega_{xy}(\mathbf{k}) = \sum_{n<E_F} \sum_{m\neq n} 2\text{Im} \frac{\langle\psi_{n\mathbf{k}}|v_x|\psi_{m\mathbf{k}}\rangle\langle\psi_{m\mathbf{k}}|v_y|\psi_{n\mathbf{k}}\rangle}{(\varepsilon_{m\mathbf{k}} - \varepsilon_{n\mathbf{k}})^2} \quad (2)$$

is the Berry curvature of occupied states with $\psi_{n\mathbf{k}}$ as the Bloch states with corresponding energies $\varepsilon_{n\mathbf{k}}$, and v_i is the ith Cartesian component of the velocity operator. The results of our calculations for $\sigma_{3\times3}^{AH}$, presented in Fig. 4 as a function of the substrate thickness, indicate a sizeable AHE in the (3×3) spin lattice state with the magnitude similar to that of bulk transition-metal ferromagnets [59–61] and much larger than that observed in bulk oxides [51–58]. The large variation of

FIG. 3. (Color online) (a) Side view and (b) top view of the proposed atomic-scale (3×3) spin lattice. Two unit cells are shown.
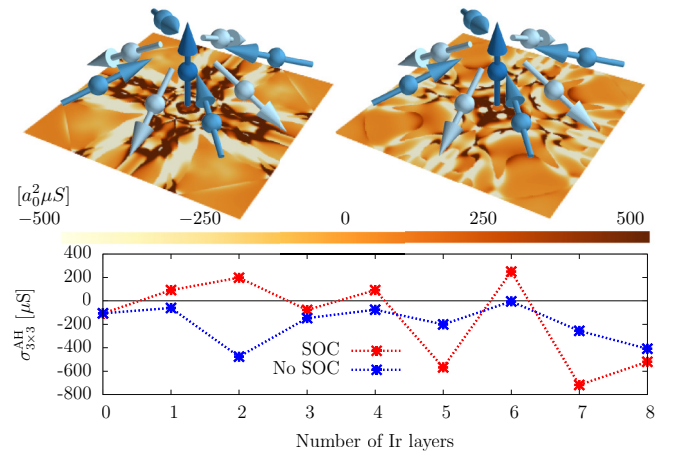

FIG. 4. (Color online) Top: BZ distribution of the Berry curvature without (left) and with (right) SOC for Fe monolayer in (3×3) state with one layer of Ir substrate, superimposed with the real-space distribution of the spins (blue arrows). Bottom: Calculated values of $\sigma_{3\times3}^{AH}$ as function of the Ir substrate thickness.

the AHC with thickness, apparent from Fig. 4, is typical for such effects as the AHE, spin Hall effect, or the spin-orbit torque in the limit of ultrathin films [60,62,63].

In the context of thin magnetic layers of transition metals on paramagnetic substrates, the emergence of the large $\sigma_{3\times3}^{\mathrm{AH}}$ appears rather surprising, since the total magnetization of the system in the (3×3) state is almost vanishing. By artificially rotating the spin moments on the Fe atoms slightly away from their equilibrium directions we acquire a complete suppression of the magnetization and observe that the values of $\sigma_{3\times3}^{\mathrm{AH}}$ stay very close to those with small uncompensated magnetization. This clearly distinguishes our case from the case of the AHE in collinear magnets, which relies on nonvanishing macroscopic magnetization and the presence of SOC [59].

Another remarkable observation is that a large contribution to $\sigma_{3\times3}^{\mathrm{AH}}$ is provided even without taking the SOC into account, as apparent from Fig. 4, where the values of the intrinsic AHC, computed with the SOC explicitly switched off in our calculations, are presented in comparison with $\sigma_{3\times3}^{\mathrm{AH}}$. Since the AHE vanishes for any collinear magnetic state of our system without SOC, it allows us to define the contribution to $\sigma_{3\times3}^{\mathrm{AH}}$ without SOC as the "topological" contribution to the AHC, $\sigma_{3\times3}^{\mathrm{TH}}$, which stems purely from the spin texture in real space, and which does not rely on the presence of SOC. The particular symmetry of our system which results in nonvanishing $\sigma_{3\times3}^{\mathrm{TH}}$ also gives rise to a finite local scalar spin chirality $\mathbf{M}_i \cdot (\mathbf{M}_j \times \mathbf{M}_k)$, nonvanishing when integrated over the unit cell [56]. To distinguish our case from the case of large two-dimensional skyrmions and bulk frustrated oxides, for which topological contribution to the Hall effect in some cases can be described neglecting the spin-orbit effects [13,14,55–57], for our class of systems we call the corresponding anomalous Hall effect without SOC the *surface topological Hall effect*. Our calculations suggest the existence of surface THE in transition-metal multilayers.

Ultimately, the large values of $\sigma_{3\times3}^{\mathrm{TH}}$ are due to a direct effect of the nontrivial real-space distribution of spin on reciprocal-space distribution of the AHC, given by the Berry curvature [64]. To convince ourselves of this explicitly, we plot in Fig. 4 the Brillouin zone distribution of the Berry curvature computed with and without SOC for the system of an Fe layer in the (3×3) spin state on one layer of the Ir substrate. As apparent from the case without SOC, there is a very close correlation of the Berry curvature distribution with the spin-distribution in real-space, while the effect of SOC is to provide an additional fine structure to this distribution stemming from SOC-induced band splittings in the vicinity of the Fermi level. Thus the surface THE is more complex than the THE in large-scale skyrmions for which the topological contribution to the THE—the emergent field—can be separated from the electronic effects in a collinear host encoded in R^{top} [10,14]. The surface THE arises from a close intertwining of the real and reciprocal space topology, which together play a role of a single multidimensional topological object with nontrivial transport properties.

The microscopic origin of the competition between non-collinearity and spin-orbit interaction for the AHE in such nontrivial surface spin textures as considered here presents an exciting direction to study both theoretically and experimentally [65,66]. In particular, we conjecture that the surface THE is commonly an important part of the AHE exhibited by complex spin structures at surfaces, such as nanoskyrmions [16]. One of its prominent manifestations would be the contribution to the orbital magnetization at the surface which does not originate in spin-orbit coupling [58,67]. The orbital magnetization and the Hall effect have the same symmetry and indeed, our calculations reveal the formation of nonvanishing local atomic orbital moments at the surface of our system without spin-orbit. Without SOC, the magnitude of the maximal local orbital moment among the Fe atoms ranges from $-0.13\,\mu_B$ to $0.03\,\mu_B$ depending on the substrate thickness, which is similar in magnitude to that obtained with spin-orbit interaction included. At the same time, the total orbital moment as a function of substrate thickness, obtained as a sum over all atomic contributions in the system, ranges from $-0.07\,\mu_B$ to $+0.04\,\mu_B$ when the SOC is not considered, which is to be compared to the range of $-0.13\,\mu_B$ to $+0.13\,\mu_B$ for the total orbital moment with SOC. Noticeably, the values of the total orbital moment without SOC are by far dominated by the contribution from the magnetic overlayer. Intuitively, this phenomenon can be understood from a simple picture in which the effect of the noncollinear environment of a given spin is similar to that of an effective spin-dependent magnetic field, which couples to orbital degrees of freedom and gives rise to the orbital moment. Such "topological" orbital magnetization could be readily addressed experimentally by surface techniques.

---

[1] N. Nagaosa and Y. Tokura, Nat. Nanotechnol. **8**, 899 (2013).

[2] K.-S. Ryu, L. Thomas, S.-H. Yang, and S. Parkin, Nat. Nanotechnol. **8**, 527 (2013).

[3] S. Emori, U. Bauer, S.-M. Ahn, E. Martinez, and G. S. D. Beach, Nat. Mater. **12**, 611 (2013).

[4] M. Hayashi, L. Thomas, R. Moriya, C. Rettner, and S. S. P. Parkin, Science **320**, 209 (2008).

[5] N. Kiselev, A. N. Bogdanov, R. Schäfer, and U. K. Rößler, J. Phys. D **44**, 392001 (2011).

[6] A. Fert, V. Cros, and J. Sampaio, Nat. Nanotechnol. **8**, 152 (2013).

[7] J. Sampaio, V. Cros, S. Rohart, A. Thiaville, and A. Fert, Nat. Nanotechnol. **8**, 839 (2013).

[8] I. E. Dzyaloshinskii, Sov. Phys. JETP **5**, 1259 (1957).

[9] T. Moriya, Phys. Rev. **120**, 91 (1960).

[10] A. Neubauer, C. Pfleiderer, B. Binz, A. Rosch, R. Ritz, P. G. Niklowitz, and P. Böni, Phys. Rev. Lett. **102**, 186602 (2009).

[11] S. X. Huang and C. L. Chien, Phys. Rev. Lett. **108**, 267201 (2012).

[12] N. Kanazawa, Y. Onose, T. Arima, D. Okuyama, K. Ohoyama, S. Wakimoto, K. Kakurai, S. Ishiwata, and Y. Tokura, Phys. Rev. Lett. **106**, 156603 (2011).

[13] P. Bruno, V. K. Dugaev, and M. Taillefumier, Phys. Rev. Lett. **93**, 096806 (2004).

[14] C. Franz, F. Freimuth, A. Bauer, R. Ritz, C. Schnarr, C. Duvinage, T. Adams, S. Blügel, A. Rosch, Y. Mokrousov *et al.*, Phys. Rev. Lett. **112**, 186601 (2014).

[15] J. Gayles, F. Freimuth, T. Schena, G. Lani, P. Mavropoulos, R. Duine, S. Blügel, J. Sinova, and Y. Mokrousov, arXiv:1503.04842 [Phys. Rev. Lett. (to be published)].

[16] S. Heinze, K. von Bergmann, M. Menzel, J. Brede, A. Kubetzka, R. Wiesendanger, G. Bihlmayer, and S. Blügel, Nat. Phys. **7**, 713 (2011).

[17] B. Dupé, M. Hoffmann, C. Paillard, and S. Heinze, Nat. Commun. **5**, 4030 (2014).

[18] B. Dupé, G. Bihlmayer, S. Blügel, and S. Heinze, arXiv:1503.08098.

[19] M. Heide, G. Bihlmayer, and S. Blügel, Physica B **404**, 2678 (2009).

[20] M. Menzel, Y. Mokrousov, R. Wieser, J. E. Bickel, E. Vedmedenko, S. Blügel, S. Heinze, K. von Bergmann, A. Kubetzka, and R. Wiesendanger, Phys. Rev. Lett. **108**, 197204 (2012).

[21] N. Romming, C. Hanneken, M. Menzel, J. E. Bickel, B. Wolter, K. von Bergmann, A. Kubetzka, and R. Wiesendanger, Science **341**, 636 (2013).

[22] X. Zhang, Y. Zhou, and M. Ezawa, arXiv:1504.01198.

[23] J. Barker and O. Tretiakov, arXiv:1505.06156.

[24] H. V. Gomonay and V. M. Loktev, Phys. Rev. B **81**, 144427 (2010).

[25] S.-H. Yang, K.-S. Ryu, and S. Parkin, Nat. Nanotechnol. **10**, 221 (2015).

[26] V. Martin, W. Meyer, C. Giovanardi, L. Hammer, K. Heinz, Z. Tian, D. Sander, and J. Kirschner, Phys. Rev. B **76**, 205418 (2007).

[27] E. Simon, K. Palotàs, L. Ròzsa, L. Udvardi, and L. Szunyogh, Phys. Rev. B **90**, 094410 (2014).

[28] S. Polesya, S. Mankovsky, S. Bornemann, D. Ködderitzsch, J. Minàr, and H. Ebert, Phys. Rev. B **89**, 184414 (2014).

[29] P. E. Blöchl, Phys. Rev. B **50**, 17953 (1994).

[30] G. Kresse and J. Furthmüller, Phys. Rev. B **54**, 11169 (1996).

[31] G. Kresse and D. Joubert, Phys. Rev. B **59**, 1758 (1999).

[32] See Supplemental Material at http://link.aps.org/supplemental/10.1103/PhysRevB.92.020401, which describes the details of the first-principles calculations.

[33] G. Kresse and J. Hafner, Phys. Rev. B **47**, 558 (1993).

[34] G. Kresse and J. Hafner, Phys. Rev. B **49**, 14251 (1994).

[35] G. Kresse and J. Furthmüller, Comput. Mater. Sci. **6**, 15 (1996).

[36] J. P. Perdew, J. A. Chevary, S. H. Vosko, K. A. Jackson, M. R. Pederson, D. J. Singh, and C. Fiolhais, Phys. Rev. B **46**, 6671 (1992).

[37] J. Kudrnovský, F. Máca, I. Turek, and J. Redinger, Phys. Rev. B **80**, 064405 (2009).

[38] J. P. Perdew and A. Zunger, Phys. Rev. B **23**, 5048 (1981).

[39] P. Ferriani, I. Turek, S. Heinze, G. Bihlmayer, and S. Blügel, Phys. Rev. Lett. **99**, 187203 (2007).

[40] J. R. Yates, X. Wang, D. Vanderbilt, and I. Souza, Phys. Rev. B **75**, 195121 (2007).

[41] A. A. Mostofi, J. R. Yates, Y.-S. Lee, I. Souza, D. Vanderbilt, and N. Marzari, Comput. Phys. Commun. **178**, 685 (2008).

[42] F. Freimuth, Y. Mokrousov, D. Wortmann, S. Heinze, and S. Blügel, Phys. Rev. B **78**, 035120 (2008).

[43] FLEUR web page; see www.flapw.de.

[44] We have obtained the following values of the exchange constants J_n between nth-nearest neighbors in the Fe monolayer on Ir(001): $J_1...J_6 = -9.44, -4.06, -1.59, -0.51, 0.01, 0.18$ meV. Note that we can only determine the value $J_3 + 0.5B = -1.59$ meV from the fitting where B is the nearest-neighbor biquadratic exchange interaction.

[45] F. Máca, J. Kudrnovský, V. Drchal, and J. Redinger, Phys. Rev. B **88**, 045423 (2013).

[46] We have checked the influence of the Ir film thickness on the energy dispersion of spin spirals up to 15 Ir layers and found convergence of the exchange parameters for 11 Ir layers.

[47] K. von Bergmann, S. Heinze, M. Bode, E. Y. Vedmedenko, G. Bihlmayer, S. Blügel, and R. Wiesendanger, Phys. Rev. Lett. **96**, 167203 (2006).

[48] A. Deák, L. Szunyogh, and B. Ujfalussy, Phys. Rev. B **84**, 224413 (2011).

[49] A. Crépieux and C. Lacroix, J. Magn. Magn. Mater. **182**, 341 (1998).

[50] M. Bode, M. Heide, K. von Bergmann, P. Ferriani, S. Heinze, G. Bihlmayer, A. Kubetzka, O. Pietzsch, S. Blügel, and R. Wiesendanger, Nature (London) **447**, 190 (2007).

[51] C. Sürgers, G. Fischer, P. Winkel, and H. Löhneysen, Nat. Commun. **5**, 3400 (2014).

[52] H. Chen, Q. Niu, and A. H. MacDonald, Phys. Rev. Lett. **112**, 017205 (2014).

[53] T. Tomizawa and H. Kontani, Phys. Rev. B **80**, 100401 (2009).

[54] T. Tomizawa and H. Kontani, Phys. Rev. B **82**, 104412 (2010).

[55] Y. Machida, S. Nakatsuji, Y. Maeno, T. Tayama, T. Sakakibara, and S. Onoda, Phys. Rev. Lett. **98**, 057203 (2007).

[56] Y. Taguchi, Y. Oohara, H. Yoshizawa, N. Nagaosa, and Y. Tokura, Science **291**, 2573 (2001).

[57] Y. Machida, S. Nakatsuji, S. Onoda, T. Tayama, and T. Sakakibara, Nature (London) **463**, 210 (2010).

[58] R. Shindou and N. Nagaosa, Phys. Rev. Lett. **87**, 116801 (2001).

[59] N. Nagaosa, J. Sinova, S. Onoda, A. MacDonald, and N. Ong, Rev. Mod. Phys. **82**, 1539 (2010).

[60] P. Czaja, F. Freimuth, J. Weischenberg, S. Blügel, and Y. Mokrousov, Phys. Rev. B **89**, 014411 (2014).

[61] The values of the AHC in units of S/cm can be obtained by dividing the values in Fig. 4 by the thickness of the film, and they lie in the range between several hundreds and several thousands S/cm, depending on the thickness. For example, in the case of a 3-layer-thick Ir substrate (0.82 nm total thickness) the total AHC constitutes -98 S/cm.

[62] F. Freimuth, S. Blügel, and Y. Mokrousov, Phys. Rev. B **90**, 174423 (2014).

[63] N. H. Long, P. Mavropoulos, B. Zimmermann, D. S. G. Bauer, S. Blügel, and Y. Mokrousov, Phys. Rev. B **90**, 064406 (2014).

[64] Z. Fang, N. Nagaosa, K. S. Takahashi, A. Asamitsu, R. Mathieu, T. Ogasawara, H. Yamada, M. Kawasaki, Y. Tokura, and K. Terakura, Science **302**, 92 (2003).

[65] R. Cheng and Q. Niu, Phys. Rev. B **86**, 245118 (2012).

[66] O. Gomonay, Phys. Rev. B **91**, 144421 (2015).

[67] J. Shi, G. Vignale, D. Xiao, and Q. Niu, Phys. Rev. Lett. **99**, 197202 (2007).